MnO_x−CeO_2 Binary Oxides for Catalytic NO_x Sorption at Low Temperatures. Sorptive Removal of NO_x

Masato Machida,* Masatoshi Uto, Daisuke Kurogi, and Tsuyoshi Kijima

Department of Applied Chemistry, Faculty of Engineering, Miyazaki University, 1-1 Gakuenkibanadai Nishi, Miyazaki 889-2192, Japan

Received March 7, 2000. Revised Manuscript Received July 6, 2000

Interactions of nitrogen oxides (NO_x) with (n)MnO_x−(1 − n)CeO_2 binary oxides were studied to use them for sorptive NO_x removal at low temperatures (≃150 °C). The formation of MnO_x−CeO_2 solid solutions with the fluorite-type structure at n ≃ 0.5 was found to be quite effective in accelerating NO_x sorption from flowing mixtures of 0.08% NO, 2% O_2, and He balance (W/F = 0.24 g·s/cm^3). The cumulative NO_x uptake was increased by decreasing the reaction temperature and/or by increasing O_2 concentration, indicative of chemisorption via oxidation of NO/NO_2. In situ FT-IR diffuse reflectance spectrometry demonstrated that adsorption of NO_x as bidentate, monodentate, and ionic nitrates is responsible for the large uptake. These adsorbates are produced by oxidative adsorption, which is caused by NO oxidation to NO_2 by lattice oxygens bound to Mn and subsequent coordination to Ce in adjacent surface sites. XPS and O_2-TPD studies suggested that the active site for NO oxidation should be related to the redox of Mn and accompanying reversible sorption/desorption of lattice oxygens.

Introduction

Several NO_x-control processes using solid sorbents are now attracting much attention in the applications to automobiles and other flue gas treatment processes in oxidizing atmosphere.[1−4] The role of solid sorbents in these processes is to remove NO_x from gas exhaust and store it until the atmosphere turns to reductive, where desorption of NO_x and subsequent catalytic reduction to N_2 become possible. The use of sorbents is expected to explore the novel catalytic processes for not only separation (or concentration) but also conversion of dilute NO_x. However, the material design of NO_x sorbents for catalytic processes is not yet established so far. One conventional strategy is to add alkaline or alkaline-earth elements, such as K and Ba, to the metal oxide matrix. The resultant reactivity to NO in the presence of O_2 brings about considerable solid−gas reactions to produce nitrate precipitations. Reported NO_x sorbing materials based on this concept include Ba−Y−Cu−O,[5−7] Ba−Cu−O,[8,9] La−Ba−Sr−Cu−O,[10−13] Ba−Al_2O_3,[14] and so on. However, the problem in these systems is strong inhibition caused by coexisting CO_2 because CO_2 and NO_x are competing for the alkaline site on the solid surface.[9] Another possible way to design highly efficient NO_x sorbents is the combination of NO-oxidation catalyst and NO_2-sorbing material. On such solids, gaseous NO is oxidized to NO_2 and subsequently sorbed as nitrite or nitrate species. Since NO_2 easily adsorbs onto metal oxides at ambient temperature, components with strong basicity are not necessary. The NO_x sorbents of this concept have been already reported for MnO_2/BaO−CuO,[9] MnO_2−ZrO_2,[15,16] Pt/ZrO_2−Al_2O_3,[17] and Pd/ZrO_2.[18] However, none of these materials was studied for use at low temperatures ≤150 °C.

From a thermodynamic viewpoint, NO oxidation and sorption become favorable as the temperature decreases. Therefore, the study should be directed toward how to accelerate solid−gas reactions by introducing catalytic components. In the present study, we have developed a

* Corresponding author. TEL: +81-985-58-7312. FAX: +81-985-58-7323. E-mail: machida@material.chem.miyazaki-u.ac.jp.

(1) Arai, H.; Machida, M. *Catal. Today* **1994**, *22*, 97.
(2) Machida, M. In *Catalysis*; The Royal Society of Chemistry: Cambridge, 2000; Vol. 15, p 73.
(3) Miyoshi, N.; Matsumoto, S.; Katoh, K.; Tanaka, T.; Harada, J.; Takahashi, N.; Yokota, K.; Sugiura, M.; Kasahara, K. *SEA Pap.* 1995, *950809*.
(4) Fridell, E.; Skoglundh, M.; Johansson, S.; Westberg, B.; Törncrona, A.; Smedler, G. In *Catalysis and Automotive Pollution Control IV;* Kruse, N., Frennet, A., Basin, J. M., Eds.; Elsevier: Amsterdam, 1998; p 537.
(5) Tabata, K.; Fukui, H.; Kohiki, S.; Mizuno, N.; Misono, M. *Chem. Lett.* **1988**, 799.
(6) Mizuno, N.; Yamato, M.; Misono, M. *J. Chem. Soc., Chem. Commun.* **1988**, 887.
(7) Arakawa, T.; Adachi, G. *Mater. Res. Bull.* **1989**, *24*, 529.
(8) Machida, M.; Yasuoka, K.; Eguchi, K.; Arai, H. *J. Chem. Soc., Chem. Commun.* **1990**, 1165.
(9) Machida, M.; Ogata, S.; Yasuoka, K.; Eguchi, K.; Arai, H. *Proc. Int.* Congr. Catal. Guczi, L., Solymosi, F., Tetenyi, P., Eds.; Elsevier: Amsterdam, 1993; p 2645.
(10) Machida, M.; Murakami, H.; Kitsubayashi, T.; Kijima, T. *J. Mater. Chem.* **1994**, *4*, 1621.
(11) Machida, M.; Murakami, H.; Kitsubayashi, T.; Kijima, T. *Chem. Mater.* **1996**, *8*, 197.
(12) Machida, M.; Murakami, H.; Kitsubayashi, T.; Kijima, T. *Chem. Mater.* **1997**, *9*, 135.
(13) Machida, M.; Murakami, H.; Kitsubayashi, T.; Kijima, T. *Appl. Catal., B* **1996**, *17*, 195.
(14) Hodjati, S.; Bernhardt, P.; Petit, C.; Pitchon, V.; Kiennemann, A. *Appl. Catal., B* **1998**, *19*, 209.
(15) Eguchi, K.; Watabe, M.; Machida, M.; Arai, H. *Catal. Today* **1996**, *27*, 297.
(16) Eguchi, K.; Watabe, M.; Ogata, S.; Arai, H *Bull. Chem. Soc. Jpn.* **1995**, *68*, 1739.
(17) Eguchi, K.; Hayashi, T. *Catal. Today* **1998**, *45*, 109.
(18) Machida, M.; Yoshii, A.; Kijima, T. *Int. J. Inorg. Mater.* **2000**, 2, in press.

10.1021/cm000207r CCC: $19.00
Published on Web 09/29/2000

novel solid sorbent for low-temperature NO_x removal, which consists of MnO_x–CeO_2 solid solution with fluorite-type crystal structure. The sorption/desorption property of NO_x over the binary oxides was investigated in relation to the redox property and the reactivity of lattice oxygens. The process for the regeneration of NO_x sorbent was also studied by applying thermal swing cycles.

Experimental Section

Preparation and Characterization. Binary oxides, $(n)MnO_x$–$(1 - n)CeO_2$, were prepared by coprecipitation from aqueous solutions of nitrates. Calculated amounts of $Mn(NO_3)_2 \cdot 6H_2O$ and $Ce(NO_3)_3 \cdot 6H_2O$ (Wako Chemicals, Guaranteed reagent grade) were dissolved in distilled water. Addition of ammonia water dropwise to the solution produced precipitates, which were evaporated to dryness and subsequently calcined at 450 °C for 5 h in air.

The crystal structure of the sample was determined by powder X-ray diffraction (XRD, Shimadzu XD-D1) using monochromated Cu Kα radiation (30 kV, 30 mA). The BET surface area was obtained by measuring N_2 adsorption isotherms at −196 °C. The XPS measurement of O1s, Ce3d, and Mn2p regions was performed on a Shimadzu-Kratos AXIS-HS spectrometer with a magnesium anode (Mg Kα, 1253.6 eV) operated at 15 kV and 10 mA. The binding energy calibration was checked by line position of C1s as an internal reference (284.6 eV). The normal operating pressure in the analysis chamber was controlled to less than 10^{-6} Pa during the measurement.

Temperature-programmed desorption (TPD) of oxygen was measured in a conventional flow reactor connected to a volumetric vacuum system and to a differential evacuation system. Prior to the measurement, the sample was treated under flowing 20% O_2/N_2 mixtures at 450 °C for 1 h; this was followed by cooling to ambient temperature. After evacuation, the sample was heated from ambient temperature to 900 °C at a constant rate of 10 °C/min in a He stream (20 cm^3/min). The gas mixtures leaving the sample were analyzed by a quadrupole residual gas analyzer mass spectrometer (LEDA-MASS, Monitorr).

NO_x Reactions. The sorptive removal of NO_x was evaluated in a conventional flow system at atmospheric pressure. In this paper, the term NO_x is used to express NO/NO_2, the molar ratio of which is dependent on O_2 partial pressure and temperature. The granular sample (10–20 mesh, 0.2 g) was fixed in a quartz tube (4 mm i.d.) by packing a quartz wool at both ends of the bed. Gaseous mixtures of 0.08% NO, 0–10% O_2, and He balance were fed to the sample at $W/F = 0.24$ g·s/cm^3. The effluent gas was analyzed by online gas chromatography (GL Science model 370) with a molecular sieve 5A column and a chemiluminescence NO_x analyzer (Shimadzu NOA305). After the NO_x sorption at 30–200 °C and subsequent cooling to ambient temperature, the sample was ramped to 600 °C at the rate of 10 °C/min in a He stream (20 cm^3/min) to obtain NO_x–TPD profiles.

In situ FT-IR spectra of NO_x species adsorbed on $(n)MnO_x$–$(1 - n)CeO_2$ were recorded on a Jasco FT-IR610 spectrometer. A temperature-controllable diffuse reflectance reaction cell (Jasco DR600A) was connected to a gas flow system and a vacuum line. The sample was first outgassed in a stream of 20 vol % O_2/He at 400 °C for 1 h and then exposed to the reaction gases containing NO and/or O_2 at 30 or 150 °C for 30 min. This was followed by stepwise heating at 150–350 °C for 30 min in flowing 20 vol % O_2/He. After each treatment reflectance spectra were recorded in He stream at ambient temperature and transformed into absorption spectra by use of the Kubelka–Munk function.

Temperature swing sorption/desorption cycles of NO_x were also carried out in a flow system. An infrared image furnace (ULVAC E-25) was used for alternating the reaction temperature between sorption and desorption steps. First, the sample bed operated isothermally at 150 °C during a sorption step, and then at 500 °C during a desorption step. The end of each step was followed by prompt change of the temperature to the next step. During the temperature swing operation, a gaseous mixture of 0.08% NO, 2% O_2, and He balance was continuously fed to the granular sample (0.2 g) held in a quartz tube (4 mm i.d.) at $W/F = 0.50$ g·s/cm^3.

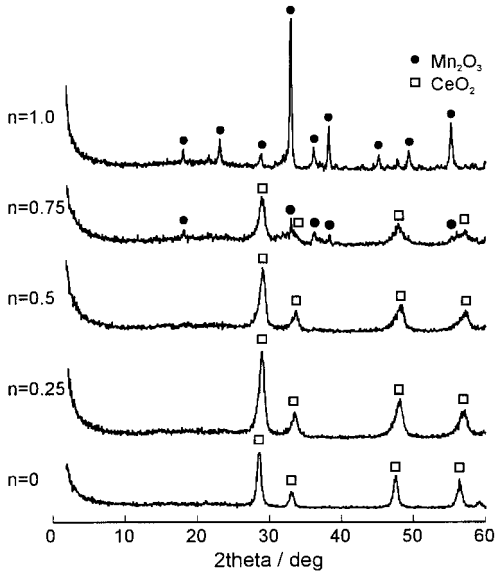

Figure 1. Powder diffraction patterns of $(n)MnO_x$–$(1 - n)$–CeO_2 after calcination at 450 °C in air.

Table 1. Composition, Lattice Parameter, and Surface Area of $(n)MnO_x$–$(1 - n)CeO_2$

n	$(Mn/Ce)^a$	$(Mn/Ce)s^b$	$a_0{}^c$/nm	surface area/m^2 g^{-1}
0.0	0.00		0.541	64.5
0.25	0.33	0.38	0.535	80.1
0.5	1.00	1.02	0.532	64.2
0.75	3.00	4.10	0.533	54.7
1.0				14.8

[a] Atomic ratio in bulk solids. [b] Atomic ratio in surface determined by XPS. [c] Lattice parameter of cubic fluorite-type phase.

Results and Discussion

Crystal Structure and Property of Lattice Oxide Ions. Figure 1 represents powder X-ray diffraction patterns of $(n)MnO_x$–$(1 - n)CeO_2$ ($0 \le n \le 1.0$) after calcination at 450 °C in air. The diffraction profiles at $n \ge 0.75$ showed the crystallization of Mn_2O_3, whereas those at $n \le 0.5$ consisted of broad reflections ascribable only to CeO_2 with a cubic fluorite structure. Heating the latter samples at 800 °C did not allow precipitation of manganese oxide phases but resulted in significant crystallization of CeO_2. However, the incremental shift of each diffraction line to higher angles suggested considerable decrease of the lattice constant from 0.541 nm ($n = 0$) to 0.532 nm ($n = 0.5$) as summarized in Table 1. These results imply the formation of solid solution between Mn_2O_3 and CeO_2. The replacement of Ce^{4+} by Mn^{3+} in the fluorite structure seems to be possible when considering their structural similarity; the crystal structure of Mn_2O_3 is the C-rare earth type that is basically composed of anion-deficient units of fluorite structure.[19] The decrease of the lattice constant with increasing n

(19) Galasso, F. G. *Structure and Properties of Inorganic Solids*; Pergamon: Oxford, 1970; p 115.

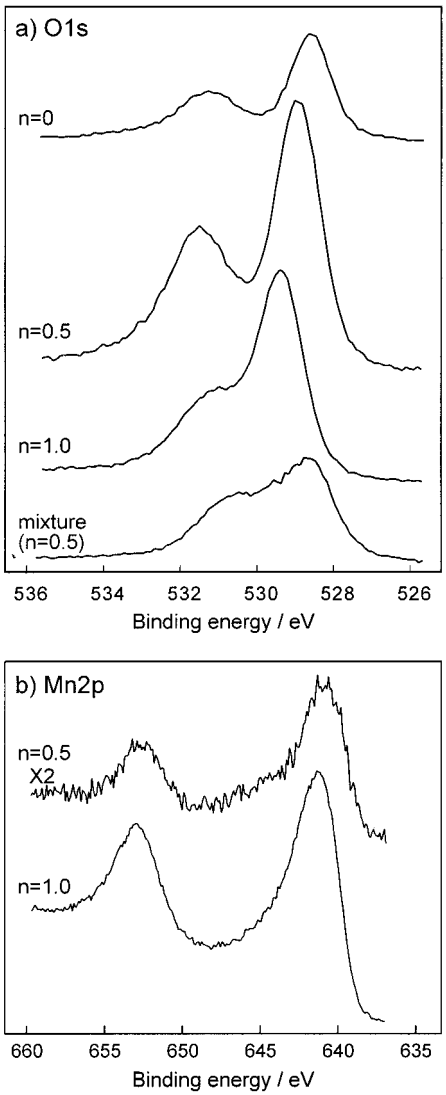

Figure 2. (a) O1s and (b) Mn2p XPS spectra of $(n)MnO_x-(1-n)CeO_2$.

is associated with the small ionic radius of Mn^{3+} (0.66 nm) as compared to Ce^{4+} (0.94 nm). From line-broadening analysis of the three strongest diffraction peaks of CeO_2, the size of crystallites is estimated to be 10.3 nm for $n = 0.5$. The calculated geometrical specific surface area (100 m^2/g) is less than the BET surface area (64.2 m^2/g) obtained from an N_2 adsorption isotherm measured at −196 °C. The disagreement is due to a considerable lattice distortion caused by forming the solid solution. As shown in Table 1, the BET surface area of CeO_2 (65.4 m^2/g) increased to 80.1 m^2/g for $n = 0.25$, whereas that of MnO_x ($n = 1.0$) was exceptionally small (16.0 m^2/g) owing to the significant grain growth of Mn_2O_3.

The XPS spectra of Mn2p, Ce3d, and O1s were measured for MnO_x ($n = 0$), MnO_x-CeO_2 ($n = 0.5$), and CeO_2 ($n = 1.0$). As given in Figure 2a, the noticeable difference was observed for O1s regions, where each signal was commonly composed of two different components. The two peak maxima at 528−530 and 531−532 eV correspond to lattice oxide ions (O^{2-}) and adsorbed carbonates, respectively. The presence of surface carbonates was supported by FT-IR measurement as described below. Here, we have noted that the position

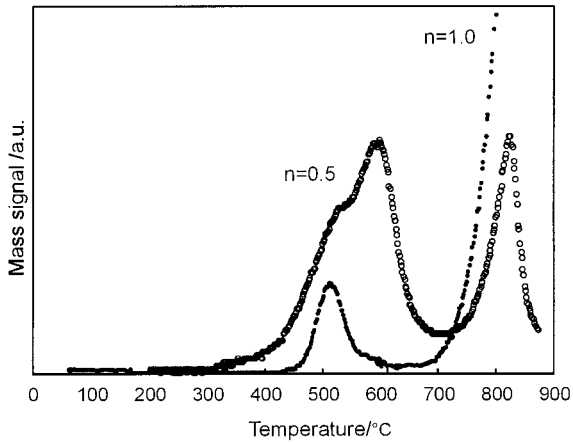

Figure 3. O_2-TPD profiles of $(n)MnO_x-(1-n)CeO_2$.

of the former component is dependent on the oxide composition. The different binding energies of two single oxides (529.4 eV for MnO_x and 528.5 eV for CeO_2) reflects the different basicity of Mn and Ce ions; i.e., oxide ions in CeO_2 seem to be more anionic than those in MnO_x. MnO_x-CeO_2 gave rise to a single O1s signal at the intermediate binding energy, 528.9 eV, which is consistent with the formation of the homogeneous solid solution between CeO_2 and Mn_2O_3. By contrast, when a physical mixture ($n = 0.5$) of these two oxides was submitted, overlapping of these two different components caused a considerable broadening of the O1s peak, which is shown as a bottom line in Figure 2a. A little chemical shift was also observed for the $Mn2p_{3/2}$ signal as shown in Figure 2b. The binding energy for MnO_x, 641.2 eV, corresponds to the reported value for Mn_2O_3,[20] whereas that for $n = 0.5$, 640.7 eV, is intermediate between Mn_2O_3 and MnO.[21] No significant changes were found for different oxide compositions in the position and the multiple splitting of the Ce3d signals. The spectra were fully consistent with that reported for CeO_2.[22] The atomic ratios Mn/Ce in the surface, which were calculated from the intensities of $Mn2p_{3/2}$ and $Ce3d_{5/2}$ signals, are compared with the bulk composition in Table 1. The ratio in the surface was nearly equal to that in the bulk at $n \leq 0.5$, reflecting the formation of homogeneous solid solutions.

TPD profiles of $(n)MnO_x-(1-n)CeO_2$ were measured to clarify the effect of solid solution formation on the reactivity of lattice oxygen. As can be seen in Figure 3, MnO_x ($n = 1.0$) showed two types of evolution peaks at 520 and <700 °C. A relatively small peak at 520 °C originates from an excess bulk oxygen in Mn_2O_3.[23] Because it is close to the decomposition temperature of bulk MnO_2, 535 °C,[24] MnO_x would contain a small amount of Mn^{4+} in the cation-deficient structure. On the other hand, a strong peak at <700 °C is attributed to the liberation of lattice oxygens from bulk Mn_2O_3 to

(20) Oku, M.; Hirokawa, K. *J. Electron Spectrosc. Relat. Phenom.* **1976**, *8*, 475.
(21) Oku, M.; Hirokawa, K.; Ikeda, S. *J. Electron Spectrosc. Relat. Phenom.* **1976**, *7*, 4.
(22) Mullins, D. R.; Overbury, S. H.; Huntley, D. R. *Surf. Sci.* **1998**, *409*, 307.
(23) Luo, M. F.; Yuan, X. X.; Zheng, Z. M. *Appl. Catal., A* **1998**, *175*, 121.
(24) *CRC Handbook of Chemistry and Physics*, 72nd ed.; Lide, D. R., Ed.; CRC Press: Boston, MA, 1991.

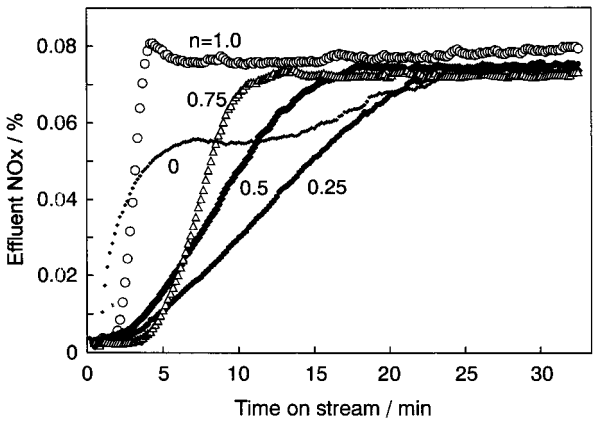

Figure 4. Effluent NO_x concentration from $(n)MnO_x$−$(1 - n)$−CeO_2 at 150 °C. 0.08% NO, 2% O_2/He, W/F = 0.24 g·s/cm^3.

produce Mn_3O_4 and subsequently MnO. Although the oxygen evolution from CeO_2 was negligible in accordance with the higher stability against reduction, the dissolution of MnO_x into the CeO_2 lattice produced a new peak at 600 °C, which was accompanied by the decrease of another peak (>700 °C) with simultaneous shift to high temperatures. The new peak should not be ascribable to the reduction of Mn^{4+} because the chemical shift observed in the Mn2p XPS spectrum in Figure 2 suggested the decreased oxidation number as compared to MnO_x ($n = 1.0$). The origin of this oxygen evolution is possibly associated with the partial reduction of Mn^{3+} to Mn^{2+} in the fluorite structure. According to the second TPD run after reoxidation in flowing O_2 at 800 °C, the sample restored the desorption peak at 600 °C, so that MnO_x−CeO_2 exhibits the redox property based on reversible soption/desorption cycles of lattice oxygens. The resultant reactivity must be more favorable than CeO_2 for the oxidation of gaseous NO.

NO_x Sorption. Sorptive NO_x removal by $(n)MnO_x$−$(1 - n)CeO_2$ was carried out in a flow reactor. Figure 4 shows the typical breakthrough curves of NO_x (NO + NO_2) at 150 °C when the mixture of 0.08% NO, 2% O_2, and He balance was used as the gas feed. In a certain period from the beginning of the reaction, neither NO_x (NO/NO_2) nor reduced products (N_2O/N_2) could be detected in the effluent; NO_x in the gas feed was therefore removed completely by sorption onto $(n)MnO_x$−$(1 - n)CeO_2$. The effluent NO_x concentration was then gradually increased up to 0.08% toward the saturation of the sorption. The cumulative NO_x uptake was obtained from these breakthrough curves measured at different temperatures and summarized in Figure 5 as a function of n in $(n)MnO_x$−$(1 - n)CeO_2$. Manganese oxides (MnO_2, Mn_2O_3) are known as active catalysts for the oxidation of NO,[9,25,26] but the NO_x uptake for $n = 1.0$ was very small. In comparison, CeO_2 ($n = 0$) showed a larger uptake compared to MnO_x because the higher basicity brings about an affinity toward NO and NO_2. The NO_x uptake was increased with an incremental fraction of MnO_x up to $n = 0.25$, where the largest surface area was obtained. The maximum uptake at 30 °C, 0.20 mmol/g, is less than the amount of Ce site (0.48 mmol/g) exposed on the surface, which is estimated by

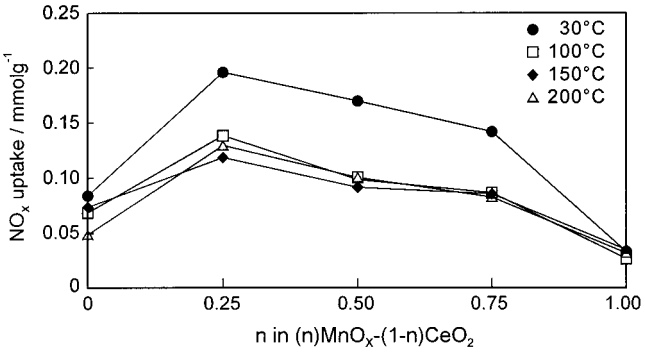

Figure 5. Cumulative NO_x uptake of $(n)MnO_x$−$(1 - n)CeO_2$ at various temperatures. 0.08% NO, 2% O_2/He, W/F = 0.24 g·s/cm^3.

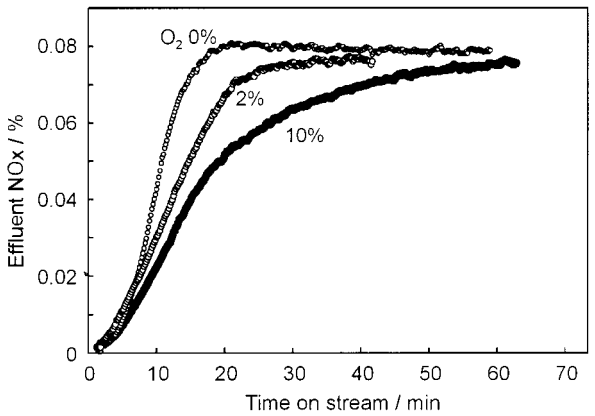

Figure 6. Effect of O_2 concentration on NO_x removal over MnO_x−CeO_2($n = 0.5$) at 150 °C. 0.08% NO, 0−10% O_2/He, W/F = 0.24 g·s/cm^3.

assuming the (110) surface of the fluorite-type structure. The surface NO_x/Ce ratio was therefore close to unity for $n = 0.5$. This means that NO_x removal in the present system should be caused mainly by adsorption onto the surface. The NO_x sorption was also examined for a physical MnO_x/CeO_2 mixture with an apparent composition of $n = 0.25$, but the NO_x uptake (0.068 mmol/g at 150 °C) was less than half of that attained by the corresponding solid solution (0.15 mmol/g). Figure 6 shows the effect of O_2 concentration (0−10%) on the NO_x breakthrough curve for MnO_x−CeO_2 ($n = 0.5$) at 150 °C. Although the sorption was observed even in the absence of O_2, the uptake was increased in the presence of O_2 with higher concentrations. The similar tendency was confirmed at different reaction temperatures from 30 to 200 °C, suggesting the sorption route via oxidation of NO to NO_2. This is consistent with the effect of reaction temperature (Figure 5) because the formation of NO_2 is thermodynamically favorable at lower temperatures. However, the considerable NO_x uptake even in the absence of O_2 (Figure 6) implies that the lattice oxygens in the MnO_x−CeO_2 solid solution play a key role in the oxidative sorption of NO.

Infrared Spectra of Sorbed NO_x. Infrared spectra covering the range 1000−2000 cm^{-1} were recorded to elucidate the chemical structure of NO_x species adsorbed on $(n)MnO_x$−$(1 - n)CeO_2$. Figure 7 compares the spectra obtained for $n = 0$, 0.5, and 1.0 after outgassing in a 20% O_2/He flow at 400 °C and subsequent exposure to a stream of He containing 0.08% NO and 2% O_2 at 30 °C. The background spectrum of CeO_2 ($n = 0$) contains

(25) Hirao, Y.; Yokoyama, C.; Misono, M. *J. Chem. Soc., Chem. Commun.* **1996**, 597.
(26) Ueda, A.; Haruta, M. *Appl. Catal., B* **1998**, *18*, 115.

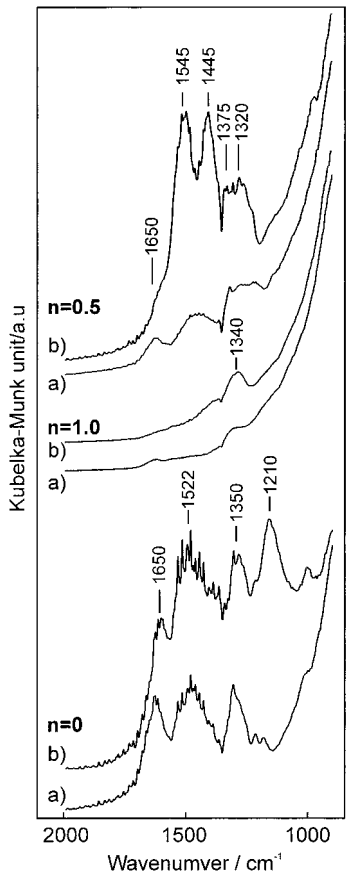

Figure 7. In situ FT-IR spectra of $(n)MnO_x-(1-n)CeO_2$ (a) before and (b) after exposure to 0.08% NO, 2% O_2/He at 30 °C.

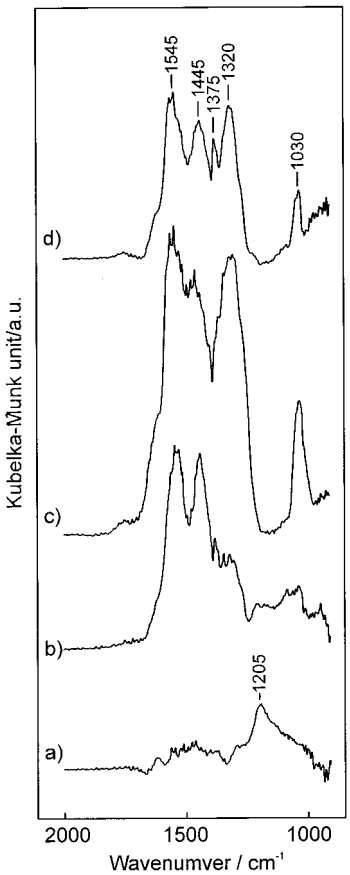

Figure 8. In situ FT-IR differencial spectra of MnO_x-CeO_2 ($n = 0.5$) after exposure to (a) 0.08% NO/He at 30 °C, (b) 0.08% NO, 2% O_2/He at 30 °C, (c) 0.08% NO, 10% O_2/He at 30 °C, and (d) 0.08% NO, 2% O_2/He at 150 °C.

bands at 1650, 1522, and 1350 cm^{-1} of residual carbonates,[27] which appear to originate from adsorption of atmospheric CO_2. Even after heating at 400 °C, the carbonates were strongly bound to the surface of CeO_2, whereas those on MnO_x-CeO_2 ($n = 0.5$) were mostly removed. The different thermal stabilities of carbonates were also supported by TPD measurement of CO_2; i.e., MnO_x-CeO_2 allowed almost complete desorption of carbonates at ca. 500 °C, compared to >700 °C required for CeO_2. The spectra taken after NO_x sorption onto these three samples were completely different in accord with the NO_x sorbability as shown in Figures 4 and 5. A band at 1210 cm^{-1} observed for CeO_2 may be ascribable to nitrite ions (NO_2^-). On MnO_x a weak band at 1340 cm^{-1} resulted from the formation of nitrate ions (NO_3^-). By contrast, the spectrum obtained for MnO_x-CeO_2 was characterized by three strong bands at 1545, 1445, and 1375 cm^{-1}, which can be assigned to bidentate and monodentate nitrates covalently bonded to surface Ce^{4+} ions. The spectrum also includes a band of ionic nitrate (NO_3^-, ca. 1320 cm^{-1}) overlapping with the third band of the covalent nitrates. These assignments are consistent with those reported previously by several researchers.[27-32] Since these bands were not detected over CeO_2 alone, new sites available for nitrate-type adsorption should be produced on the surface of MnO_x-CeO_2 solid solutions. Figure 8a–c represents the differential spectra of MnO_x-CeO_2 ($n = 0.5$) after exposure to NO mixtures with various O_2 concentrations. Sorption at 30 °C in the absence of O_2 generated a nitrite band at 1205 cm^{-1} together with very weak nitrate bands (a). Adding O_2 in the gas feed drastically changed the structure of adsorbates in a concentration-dependent manner. The sorption in the presence of 2% O_2 generated two strong bands at 1545 and 1440 cm^{-1} (bidentate and monodentate nitrates) and smaller bands at 1350 and 1125 cm^{-1} (ionic nitrate) with simultaneous disappearance of the nitrite band (b). Although these three nitrate bands increased in intensity upon NO_x sorption in the presence of 10% O2, the most prominent increase was observed for the band ascribable to ionic nitrate (c). The incremental formation of ionic nitrate was also observed when the temperature raised to 150 °C with O_2 concentration kept at 2% (d).

To evaluate the thermal stability of NO_x sorbed onto MnO_x-CeO_2, the spectra were also recorded after exposure to mixtures of 0.08% NO, 2% O_2, and He at 30 °C and subsequent heating in a He flow at progressively increasing temperatures (Figure 9a–d). Heating at 150 °C increased the intensity of nitrate bands (b) despite the decreased NO_x uptake as shown in Figure 5. This should be due to a conversion of physisorption or weak

(27) Nakamoto, K. *Infrared and Raman Spectra of Inorganic and Coordination Compounds*, 4th ed.; Wiley: New York, 1986.
(28) Pena, M. A.; Tascon, J. M. D.; Fierro, J. L. G.; Tejuca, L. G. *J. Colloid Interface Sci.* **1987**, *119*, 100.
(29) London, J. W.; Bell, A. T. *J. Catal.* **1973**, *31*, 32.
(30) Rochester, C. H.; Tppham, S. A. *J. Chem. Soc., Faraday Trans.* **1979**, *75*, 872.
(31) Busca, G.; Lorenzelli, V. *J. Catal.* **1981**, *72*, 303.
(32) Low, M. J. D.; Yang, R. T. *J. Catal.* **1974**, *34*, 479.

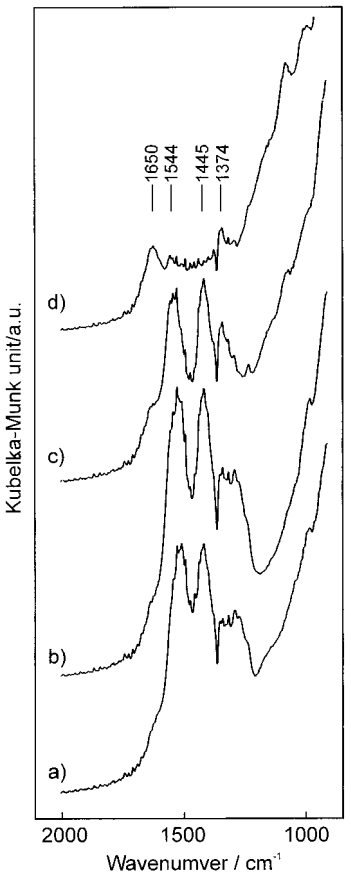

Figure 9. In situ FT-IR spectra of MnO_x−CeO_2 (a) after exposure to 0.08% NO, 2% O_2/He at 30 °C and subsequent heating at (b) 150 °C, (c) 250 °C, and (d) 350 °C in a He flow.

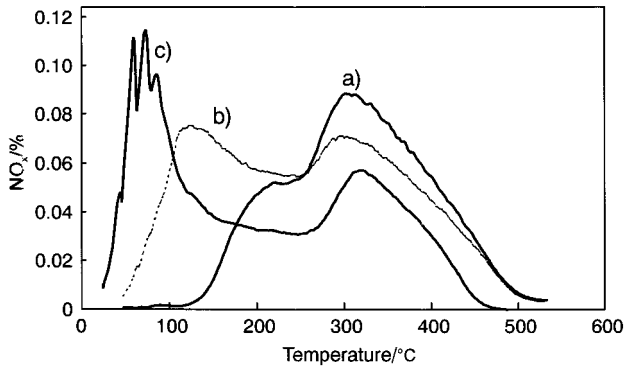

Figure 10. NO_x−TPD profiles of MnO_x-CeO_2 (n = 0.5) after exposure to (a) 0.08% NO, 2% O_2/He at 150 °C, (b) 0.08% NO, 2% O_2/He at 30 °C, and (c) 0.08% NO/He at 30 °C, for 1 h.

chemisorption into nitrate adsorbates. After heating at 250 °C, however, bands of bidentate and monodentate nitrate decreased in intensity (c), whereas those of ionic nitrate partly remained even at <300 °C, indicative of the higher thermal stability. Almost all bands originating from NO_x sorption disappeared after heating at 350 °C for 1 h, leaving weak bands at 1650 and 1370 cm^{-1} ascribable to residual carbonates.

NO_x Desorption. The desorption property of NO_x from MnO_x-CeO_2 (n = 0.5) was studied by means of TPD. Figure 10 shows desorption profiles of NO_x sorbed under various conditions. When the sorption was carried out at 150 °C in the presence of O_2 (2%), two desorption peaks were observed at 200 and 290 °C (a), which are

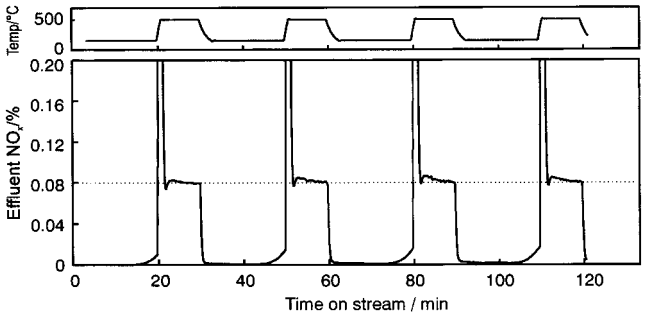

Figure 11. Temperature swing NO_x sorption/desorption cycles over MnO_x−CeO_2 (n = 0.5): 0.08% NO, 2% O_2/He, W/F = 0.50 g·s/cm^3.

attributable to bidentate/monodentate nitrates and ionic nitrate, respectively, as judged from comparison with FT-IR results (Figure 8). The NO_x sorption at lower temperatures not only decreased the intensity of the ionic nitrate peak but also generated another strong peak at ca. 120 °C (b), which would be attributed to the weakly bound nitrite species. The nitrite peak with a considerable amount of desorption is in good agreement with the difference of isothermal NOx uptakes at 30 and 150 °C (Figure 5). When the NO_x sorption was carried out at 30 °C in the absence of O_2, the desorption peak due to the weakly bound NO_x species further increased in intensity with simultaneous shift to lower temperatures (c). The adsorbate in this case, however, is not mostly detectable by FT-IR measurement probably because of very weak interactions with the surface.

Since desorption of NO_x can be completed at 500 °C in all above cases, the MnO_x−CeO_2 (n = 0.5) was next applied to temperature swing sorption/desorption cycles in a flow reactor. In this measurement, isothermal heating at 150 °C for a sorption step and at 500 °C for a desorption step was repeated with supplying gas mixtures of 0.08% NO, 2% O_2, and He balance. The result is shown in Figure 11 as the change of NO_x (NO + NO_2) concentration in the effluent gas during the temperature swing cycles. In the sorption step, almost complete sorptive removal of NO_x continued about 15 min. At the end of each sorption step, the temperature was raised to 500 °C and NO_x stored in the solid was immediately condensed out of the stream. The reversible sorption/desorption cycles could be maintained with no signs of deactivation.

Effect of Formation of Solid Solution on NO_x Sorption. The present study has revealed that the appreciable enhancement in NO_x sorbability was attained by forming the MnO_x−CeO_2 solid solution with fluorite structure. As was evident from in situ FT-IR results (Figure 7), the large NO_x uptake is clearly reflected by the different types of NO_x adsorbates. Although CeO_2 with medium basicity is expected to show some affinity to NO, the sorption onto CeO_2 alone produced only a small amount of nitrite (NO_2^-) even in the presence of coexisting O_2. This is explained by the low activity of CeO_2 for oxidation of NO/NO_2. The formation of nitrates was detected on MnO_x (Mn_2O_3) having excellent activity for NO oxidation, whereas the amount of NO_x sorption was very small probably because of the acidic character and the low specific surface area. In complete contrast to these single oxides, MnO_x−CeO_2 solid solution produced a large amount of

bidentate, monodentate, and ionic nitrates in the presence of O_2. The considerable formation of these oxidized adsorbates is explained by the fact that the solid solution possesses the combination of NO_x oxidation activity and moderate basicity, yielding significant synergism in NO_x sorbability. These results provide some evidence to support that NO_x sorption in the presence of O_2 proceeded through the oxidation of NO to nitrite and then to nitrate. It seems that the oxidation activity is closely related to the redox property of Mn and resulting reversible lattice oxygens as was revealed by XPS and O_2-TPD. Gaseous NO would first react with surface oxygens bound to Mn to form NO_2 adsorbates, which would then coordinate to a $Ce^{4+}-O^{2-}$ pair in an adjacent site to produce monodentate or bidentate nitrate complexes. Manganese thus reduced should be oxidized readily by gaseous O_2; otherwise, the formation of nitrate adsorbates would not proceed. Part of the adsorbed nitrates would also take part in conversion into ionic nitrate (NO_3^-), which is favored at high O_2 concentrations and at elevated temperatures. In these processes, the random distribution of Mn and Ce in the fluorite lattice appears to be effective in producing a large number of pair sites for oxidative sorption. According to this mechanism through such on-site catalytic NO oxidation, the NO_x sorption will proceed more efficiently in the presence of gaseous O_2. But, the sorption should be completed when the nitrate coordination onto all the cerium ions on the surface is to be saturated. This was supported by the 1:1 correspondence between adsorbed NO_x molecules and the cerium site on the surface of MnO_x-CeO_2 ($n = 0.5$).

Conclusion

The present study showed the excellent NO_x sorbability of the MnO_x-CeO_2 system at low temperatures (<150 °C). The NO_x-trapping capacity of the present system is related to the adjacent pair site with different characters, i.e., NO_x oxidation activity and NO_x sorbability, which is created on the surface of the homogeneous solid solution. Unlike the reported sorbing materials based on nitrate precipitation via solid−gas reactions, NO_x adsorbates on MnO_x-CeO_2 could be desorbed at relatively low temperatures (<350 °C), so that resultant high reactivity is expected toward various reducing agents, such as H_2, CO, and/or hydrocarbons. In the next step of this series of studies, therefore, we are studying the catalytic use of this NO_x-sorbing material, especially for selective NO_x reduction in strongly oxidizing atmosphere.

Acknowledgment. The present study was supported by Iketani Science Foundation and Grant-in Aid for Scientific Research from the Ministry of Education, Science, Sports, and Culture.

CM000207R